

Impact of Pointing Error on Coverage Performance of 3D Indoor Terahertz Communication Systems

Zhifeng Tang*, Nan Yang*, Xiangyun Zhou*, Salman Durrani*, Markku Juntti†, and Josep Miquel Jornet‡

*School of Engineering, Australian National University, Canberra, ACT 2600, Australia

†Centre for Wireless Communications, University of Oulu, Oulu 90014, Finland

‡Department of Electrical and Computer Engineering, Northeastern University, Boston, MA 02120, USA

Emails: {zhifeng.tang, nan.yang, xiangyun.zhou, salman.durrani}@anu.edu.au,
markku.juntti@oulu.fi, j.jornet@northeastern.edu

Abstract—In this paper, we develop a tractable analytical framework for a three-dimensional (3D) indoor terahertz (THz) communication system to theoretically assess the impact of the pointing error on its coverage performance. Specifically, we model the locations of access points (APs) using a Poisson point process, human blockages as random cylinder processes, and wall blockages through a Boolean straight line process. A pointing error refers to beamforming gain and direction mismatch between the transmitter and receiver. We characterize it based on the inaccuracy of location estimate. We then analyze the impact of this pointing error on the received signal power and derive a tractable expression for the coverage probability, incorporating the multi-cluster fluctuating two-ray distribution to accurately model small-scale fading in THz communications. Aided by simulation results, we corroborate our analysis and demonstrate that the pointing error has a pronounced impact on the coverage probability. Specifically, we find that merely increasing the antenna array size is insufficient to improve the coverage probability and mitigate the detrimental impact of the pointing error, highlighting the necessity of advanced estimation techniques in THz communication systems.

Index Terms—Terahertz communications, pointing error, stochastic geometry, coverage probability.

I. INTRODUCTION

Terahertz (THz) communications has emerged as a promising solution for the sixth generation wireless systems to meet the growing demands for ultra-high-speed and high-capacity wireless connectivity [1]. Specifically, THz communications operate within the 0.1–10 THz frequency range, offering abundant spectrum resources and ultra-short symbol durations [2]. However, several technical challenges hinder its widespread adoption, including severe spreading loss, molecular absorption, and sensitivity to blockages [3]. To unlock the potential of THz technology for next-generation wireless systems, it is essential to address the challenges through comprehensive system analysis, optimization based design [4].

Recent studies have evaluated the performance of THz communication systems while accounting for the unique characteristics of THz channels [5]–[10]. In particular, [5] analyzed the impacts of human blockages on signal propagation and derived a closed-form expression for the coverage probability. In [6], a Taylor series approximation was employed to examine the interference and coverage probability in THz communication systems. The impact of wall blockages on the coverage performance was examined in [7], emphasizing

their significance in indoor environments. Furthermore, [8] investigated the joint impact of human and wall blockages on the coverage performance of a three-dimensional (3D) THz communication system. Similarly, [9] assessed this joint impact on the coverage probability and average transmission rate in integrated sub-6 GHz and THz systems. More recently, [10] incorporated a fluctuating two-ray (FTR) model to accurately capture small-scale fading characteristics and analyzed the impact of user location on coverage performance in indoor environments.

It is worth noting that most of these studies have relied on high-directional antennas to mitigate path loss and enhance signal power in THz communication systems. While such antennas improve directivity and beamforming capabilities, they are highly susceptible to transceiver misalignment, known as pointing error, which significantly degrades system performance [11], [12]. Therefore, several studies have analyzed the impacts of the pointing error on system performance in various THz communications scenarios. For instance, [13] introduced an analytical framework to evaluate the pointing error in THz links, providing fundamental insights into the severity of the pointing error. Building on this, [14] proposed an analytical pointing error model for highly directional THz transmissions, facilitating performance evaluation in practical deployments. Additionally, [15] examined the impact of the pointing error on the outage probability in an unmanned aerial vehicle (UAV)-assisted communications system and proposed optimization algorithms to ensure robust connectivity in the presence of mobility-induced misalignment. While these studies provide valuable insights into the pointing error in various cases, its impact on the coverage performance in indoor THz communication systems has not been adequately evaluated, which motivates this work.

In this paper, we introduce a tractable analytical framework to precisely assess the impact of the pointing error on the coverage probability in indoor THz communication systems. We model the locations of access points (APs) using a Poisson point process, human blockages as a random cylinder process, and wall blockages through a Boolean straight-line process. The pointing error is characterized by location estimation inaccuracies between the transmitter and receiver. Focusing on this system model, we first analyze the impact of the pointing error on the received signal and then employ stochastic geometry

to derive a tractable expression for the coverage probability. Aided by simulations, we demonstrate the accuracy of our analytical results and reveal the substantial impact of pointing errors on coverage performance, highlighting that coverage probability is fundamentally limited by the pointing error and cannot be indefinitely improved by merely increasing the antenna array size.

II. SYSTEM AND CHANNEL MODEL

A. System Deployment

We consider a generalized 3D indoor THz communication system, where multiple APs mounted on the ceiling transmit THz signals to user equipment (UEs). Specifically, we assume that the ceiling has a fixed height h_A in the indoor environment and the locations of THz APs follow a Poisson point process (PPP) with the density of λ_A . We also assume that UEs, having a fixed height h_U , are randomly distributed on the ground. In this system, we randomly select one UE and refer to it as the typical UE, denoted by U_0 .

We consider that the blockage of a transmission link is caused by both human bodies and wall blockages. Following state-of-the-art studies [7], [10], we model each human body as a cylinder with a radius of R_B and a height of h_B . The bottom center of these cylinders is modeled by a 2D-PPP with the density λ_B . As illustrated in [10, Fig. 3], if the bottom center of a human body lies within the line-of-sight (LoS) blockage zone, the AP-UE signal transmission link is blocked. Conversely, if a human body is entirely outside the LoS blockage zone, the AP-UE link is considered as a LoS link, and the signal transmitted by the AP reaches the UE.

We employ the tractable Boolean scheme of straight lines to model wall blockages in the indoor environment, as in [8]. We assume that the length of walls, L_W , follow an arbitrary probability density function (PDF) of $f_{L_W}(L_W)$ with the mean $\mathbb{E}[L_W]$, and the centers of walls form a PPP with a density of λ_W . We ignore the widths of the walls, as their widths are much smaller compared to their lengths. Also, we assume that the orientations of the walls are binary, taking values of either 0 or $\pi/2$ with equal probability, ensuring that the walls are either parallel or orthogonal to each other. Finally, we assume that the height of walls is fixed and equals the height of the APs, i.e., $h_W = h_A$.

According to [7], [8], the probability that an AP-UE link is not blocked by human bodies and wall blockages is given by $p_{H,\text{LoS}}(d) = \exp(-\alpha d)$ and $p_{W,\text{LoS}}(d) = \exp(-\eta d)$, respectively, where $\alpha \triangleq 2\lambda_B R_B (h_B - h_U)/(h_A - h_U)$, $\eta = \frac{2\lambda_W \mathbb{E}[L_W]}{\pi}$, and d is the horizontal distance between the AP and the UE. Thus, the probability that an AP-UE link is not blocked is given by $p_{\text{LoS}}(d) = p_{H,\text{LoS}} p_{W,\text{LoS}} = \exp(-(\alpha + \eta)d)$.

In the considered system, we adopt the nearest-LoS-AP association strategy, i.e., each UE associates with its nearest AP that has a LoS propagation path to it. For the typical UE, we denote its associated AP by AP_0 and the horizontal distance between U_0 and AP_0 by d_0 . For other LoS non-associated APs, we denote AP_i as the i th nearest LoS non-

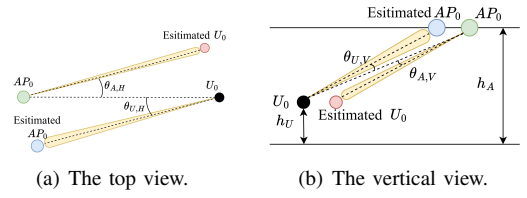


Fig. 1. Top and vertical views of the pointing error for an AP-UE link. associated AP of U_0 and d_i as the distance between U_0 and AP_i , where $\Psi_{AP} = \{AP_1, AP_2, \dots\}$.

B. Antenna Model

We assume that both APs and UEs are equipped with planar antennas to enhance signal strength to compensate for the severe path loss in THz propagation [16]. Specifically, each AP is equipped with an $N_A \times N_A$ planar antenna array, while each UE is equipped with an $N_U \times N_U$ planar antenna array, both with an element spacing of $z = \frac{\lambda}{2}$, to achieve narrow beamwidth and high antenna gain. According to [13], the antenna gain in the direction of the elevation angle θ_q and azimuth angle ϕ_q is given by $G_q(\theta_q, \phi_q) = G_{q,\text{max}} H_{pe,q}(\theta_q, \phi_q)$, where $G_{q,\text{max}} \approx \pi N_q^2$ represents the maximum antenna gain, $\theta_q = \arctan(\sqrt{\tan^2(\theta_{q,V}) + \tan^2(\theta_{q,H})})$, with $\theta_{q,V}$ and $\theta_{q,H}$ representing the angles from the target direction in the horizontal and vertical plane, respectively, as shown in Fig. 1, and

$$H_{pe,q}(\theta_q, \phi_q) = \left(\frac{\sin\left(\frac{N_q \pi \sin(\theta_q) \sin(\phi_q)}{2}\right) \sin\left(\frac{N_q \pi \sin(\theta_q) \cos(\phi_q)}{2}\right)}{N_q \sin\left(\frac{\pi \sin(\theta_q) \sin(\phi_q)}{2}\right) N_q \sin\left(\frac{\pi \sin(\theta_q) \cos(\phi_q)}{2}\right)} \right)^2. \quad (1)$$

Here, $q \in \{A_i, U_i\}$, where A_i corresponds to AP_i for the AP_i-U_0 link and U_i corresponds to U_0 for the AP_i-U_0 link.

To enable signal transmission, a typical UE, U_0 , initiates this process by sending a request to its associated AP, AP_0 . Upon receiving this request, AP_0 estimates the location of U_0 and adjusts its antenna beam towards the estimated location of U_0 . Simultaneously, AP_0 transmits its relative location back to U_0 , enabling U_0 to adjust its antenna beam towards AP_0 for efficient signal reception.

C. THz Channel Model

The signal propagation at THz frequencies is affected by the distance-dependent large-scale fading and multipath-induced small-scale fading. By combining large-scale and small-scale fading models, the received power at U_0 from AP_i is expressed as

$$P_i = P_t G_i H_{L,i} H_{S,i}, \quad (2)$$

where P_t is the transmit power, $G_i = G_{i,A} G_{i,U}$ is the combined effective antenna gain, with $G_{i,A}$ and $G_{i,U}$ representing the antenna gains at AP_i and U_0 , respectively, and $H_{L,i}$ and $H_{S,i}$ denote large-scale and small-scale fading gains for the AP_i-U_0 link, respectively.

In THz communication systems, the large-scale fading is primarily determined by the spreading loss and the molecular

absorption loss. The large-scale fading gain, $H_{L,i}$, from AP_i located at the distance d_i in the 3D indoor environment is expressed as $H_{L,i} = \xi W(d_i)$, where $\xi \triangleq \frac{c^2}{(4\pi f)^2}$, $c = 3 \times 10^8$ m/s is the light speed, f is the operating frequency, $W(d_i) = \frac{1}{d_i^2 + (h_A - h_U)^2} \exp\left(-\epsilon(f)\sqrt{d_i^2 + (h_A - h_U)^2}\right)$, and $\epsilon(f)$ is the molecular absorption coefficient of frequency f .

For the small-scale fading, compared to other existing distributions, the multi-cluster FTR (MFTR) distribution is particularly well-suited for THz communications due to the dominance of LoS and single reflected paths accompanied by diffraction and scattering at THz frequencies for short-distance transmission [17]. Therefore, we model $H_{S,i}$ using the MFTR distribution. Under this model, the cumulative distribution function (CDF) of $H_{S,i}$ is given by

$$F_{H_{S,i}}(h) = 1 - \frac{m^m}{\Gamma(m)} \sum_{j=0}^{\infty} \frac{(\mu K)^j r_j}{j! \Gamma(j + \mu)} \Gamma\left(j + \mu, \frac{h}{2\sigma^2}\right), \quad (3)$$

where $\Gamma(\cdot)$ is the gamma function and $\Gamma(\cdot, \cdot)$ is the upper incomplete gamma function [18]. In (3), the parameter m characterizes the severity of fading, μ is the number of cluster, K is the average power ratio of the dominant component to the remaining diffuse multipath, $2\sigma^2 = \frac{1}{\mu(K+1)}$ is the average power of the diffuse component over MFTR fading, and r_j is given in [10, Eq.(7)], where Δ is the parameter representing dominant waves similarity in cluster 1 of MFTR and ${}_2F_1(\cdot, \cdot; \cdot; \cdot)$ is the Gauss hypergeometric function.

To analyze the downlink coverage performance of a THz communication system, we employ the coverage probability, denoted by P_c , as our performance metric. It is defined as the probability that the received signal-to-interference-plus-noise ratio (SINR) at U_0 exceeds a given threshold γ_{th} , i.e., $P_c = \Pr(\text{SINR} > \gamma_{\text{th}})$. Accordingly, the SINR of U_0 is formulated as

$$\text{SINR} = \frac{P_0}{I + N_0} = \frac{P_t \xi G_0 W(d_0) H_{S,0}}{\sum_{AP_i \in \Psi_{AP}} P_t \xi G_i W(d_i) H_{S,i} + N_0}, \quad (4)$$

where I represents the interference power from all LoS non-associated APs and N_0 denotes the noise power.

III. COVERAGE PROBABILITY ANALYSIS

In this section, we analyze the coverage probability, P_c , under the impact of the pointing error. In our considered system, the pointing error degrades the antenna gain for the AP₀- U_0 link, which consequently affects the received signal power. Therefore, we commence our analysis by evaluating the impact of the pointing error on the received signal power.

A. Pointing Error Analysis

The pointing error refers to the antenna direction mismatch between the transmitter and receiver. We note that the antenna beams of U_0 and AP₀ are supposed to be directed towards each other, i.e., $\theta_{A_0} = \theta_{U_0} = 0$, and the antenna gain of the received signal at U_0 is supposed to be equal to the maximum antenna gain. However, due to the location

estimation inaccuracy induced by pointing error, the antenna gain of the received signal at U_0 is expressed as

$$G_0 = G_{\max} H_{pe} = G_{A,\max} G_{U,\max} H_{pe}, \quad (5)$$

where $H_{pe} = H_{pe,A_0}(\hat{\theta}_{A_0}, \phi_{A_0}) H_{pe,U_0}(\hat{\theta}_{U_0}, \phi_{U_0})$ represents the pointing error loss, and $\hat{\theta}_{A_0}$ and $\hat{\theta}_{U_0}$ are estimated angle error for AP₀ and U_0 , respectively. Since the estimated angle error for AP₀ and U_0 originates from the location estimation of U_0 , we assume that both AP₀ and U_0 share the same estimated angle errors, i.e., $\hat{\theta}_{U_0} = \hat{\theta}_{A_0} = \hat{\theta}$. Also, since square antenna arrays are deployed at the AP and the UE, we assume that the array element has a symmetrical radiation pattern in the azimuth direction [13]. According to [19], we assume that the estimated angle error in the horizontal and vertical plane follows an independent and identical zero-mean Gaussian distribution with standard deviation ς_θ , i.e., $\hat{\theta}_H \sim \mathcal{N}(0, \varsigma_\theta)$ and $\hat{\theta}_V \sim \mathcal{N}(0, \varsigma_\theta)$. Given these assumptions, we derive the PDF of the pointing error loss in the following lemma.

Lemma 1: The PDF of pointing error loss, $f_{H_{pe}}(h_{pe})$, is approximated as

$$f_{H_{pe}}(h_{pe}) \approx \beta h_{pe}^{\beta-1}, \quad (6)$$

$$\text{where } \beta = \frac{1.06^2}{2\varsigma_\theta^2(N_A^2 + N_U^2)}.$$

Proof: The main lobe gain at AP₀ and U_0 can be approximated by a Gaussian beam as $H_{pe,q}(\hat{\theta}, \phi_q) \approx \exp\left(-\hat{\theta}^2/\omega_q^2\right)$, where $\omega_q = \frac{1.06}{N_q}$. Therefore, H_{pe} is approximated by

$$H_{pe} \approx \exp\left(-\frac{\hat{\theta}^2(N_A^2 + N_U^2)}{1.06^2}\right). \quad (7)$$

For small values of $\hat{\theta}_V$ and $\hat{\theta}_H$, $\hat{\theta}$ can be approximated by $\hat{\theta} = \sqrt{\hat{\theta}_V^2 + \hat{\theta}_H^2}$. Since $\hat{\theta}_V$ and $\hat{\theta}_H$ follow independent and identical Gaussian distributions, $\hat{\theta}$ follows a Rayleigh distribution. Accordingly, $\hat{\theta}^2$ follows an exponential distribution and its PDF is given by

$$f_{\hat{\theta}^2}(\Theta) = \frac{1}{2\varsigma_\theta^2} \exp\left(-\frac{\Theta}{2\varsigma_\theta^2}\right). \quad (8)$$

By combining (7) and (8), the CDF of H_{pe} is obtained as

$$F_{H_{pe}}(h_{pe}) = 1 - F_{\hat{\theta}^2}\left(-\frac{1.06^2 \ln h_{pe}}{N_A^2 + N_U^2}\right) = h_{pe}^\beta. \quad (9)$$

We then obtain $f_{H_{pe}}(h_{pe})$ by taking the derivative of $F_{H_{pe}}(h_{pe})$ with respect to h_{pe} , resulting in (6). ■

Remark 1: From Lemma 1, we find that the average antenna gain under the asymptotic condition is given by

$$\lim_{N_A \rightarrow \infty} \bar{G}_0 = \lim_{N_A \rightarrow \infty} \frac{1.06^2 \pi^2 N_A^2 N_U^2}{1.06^2 + 2(N_A^2 + N_U^2) \varsigma_\theta^2} = \frac{1.06^2 \pi^2 N_U^2}{2\varsigma_\theta^2}, \quad (10)$$

which is constrained by ς_θ and extremely lower than the maximum antenna gain of AP, which approaches infinity. It indicates that the pointing error has a significant impact on the received signal power, and in turn, impacts the coverage probability. Additionally, the expression for \bar{G}_0 reveals that the

average antenna gain decreases when the difference between N_A and N_U increases while $N_A N_U$ is kept as a constant.

B. AP Association and Interference Analysis

In this subsection, we derive the PDF of the horizontal distance from U_0 to AP_0 , $f_{D_0}(d_0)$, and evaluate the antenna gain of interference. Leveraging the properties of the PPP, the AP intensity at a horizontal distance d from U_0 is given by $\Lambda_A(d) = 2\pi d \lambda_A$. Based on this, we first derive $f_{D_0}(d_0)$ in the following Lemma.

Lemma 2: The PDF of the horizontal distance between U_0 and AP_0 , d_0 , is derived as

$$f_{D_0}(d_0) = \Lambda_{A,\text{LoS}}(d_0) e^{-\int_0^{d_0} \Lambda_{A,\text{LoS}}(d) dd}, \quad (11)$$

where $\Lambda_{A,\text{LoS}}(d_0) = \Lambda_A(d_0) e^{-(\alpha+\eta)d_0}$.

Proof: Based on the blockage model, the LoS AP intensity at a horizontal distance d from U_0 is given by $\Lambda_{A,\text{LoS}}(d) = e^{-\alpha d} \Lambda_A(d)$. Since APs are distributed according to a PPP, the probability that the number of LoS APs within the distance d from U_0 , denoted by $N_{A,\text{LoS}}(d)$, equals n is given by

$$\Pr(N_{A,\text{LoS}}(d) = n) = \frac{(\Xi(d))^n}{n!} \exp(-\Xi(d)), \quad (12)$$

where $\Xi(d) = \int_0^d \Lambda_{A,\text{LoS}}(x) dx$. Thus, the CDF of d_0 is obtained as $F_{D_0}(d_0) = 1 - \exp(-\Xi(d_0))$. By taking the derivative of $F_{D_0}(d_0)$, we obtain $f_{D_0}(d_0)$ as given in (11). \blacksquare

Based on Lemma 2, we find that the average horizontal distance between U_0 and AP_0 , d_0 , increases monotonically with both the average wall length and the density of human blockages. This indicates that greater obstruction in the environment pushes the associated AP farther from the user, due to the reduced LoS probability and increased attenuation in nearby areas.

We then analyze antenna gains of interference signals, laying the foundations for our subsequent interference analysis. The antenna gain of the transmit signal from AP_i to U_0 is the product of transmit and receive antenna gains, expressed as $G_i = G_{i,A} G_{i,U}$. To simplify the antenna gain analysis of interfering APs, we adopt the cone model proposed in [8]. We assume that the vertical and horizontal main lobe beamwidths of APs and UEs are equal to their half-power beamwidth, i.e., $\phi_{q,V} = \phi_{q,H} \approx \frac{0.886 \times 2}{N_q}$. Moreover, the antenna gains of the main lobe and the side lobes for APs and UEs are expressed as $G_q^m = \pi N_q^2$ and

$$G_q^s = \frac{\pi - N_q^2 \pi \arcsin \left(\tan \left(\frac{\phi_{q,V}}{2} \right) \tan \left(\frac{\phi_{q,H}}{2} \right) \right)}{\pi - \arcsin \left(\tan \left(\frac{\phi_{q,V}}{2} \right) \tan \left(\frac{\phi_{q,H}}{2} \right) \right)}, \quad (13)$$

respectively. Based on these assumptions, we examine transmit and receive antenna gains separately.

1) Transmit Antenna Gain: The transmit antenna gain depends on whether U_0 falls within the antenna beam of the interfering AP. We assume that the depression angle from the AP is uniformly distributed over $[\phi_{AP}, \pi/2]$, where $\phi_{AP} = \arctan \left(\frac{h_A - h_U}{R_A} \right)$ is the depression angle from the

AP to its coverage boundary with radius R_A [7]. We also assume that the horizontal beam direction from the AP is uniformly distributed over $[0, 2\pi]$. Therefore, the transmit antenna gain equals the main lobe gain with the hitting probability $p_A = p_{A,V} p_{A,H}$, where $p_{A,V} = \min \left\{ \frac{\phi_{A,V}}{\frac{\pi}{2} - \phi_{AP}}, 1 \right\}$ and $p_{A,H} = \frac{\phi_{A,H}}{2\pi}$ are the probabilities that U_0 is located within the AP's vertical beam and horizontal beam, respectively.

2) Receive Antenna Gain: The receive antenna gain depends on whether the interfering AP is within the antenna beam of U_0 . We note that the antenna beam of U_0 is oriented towards its associated AP, AP_0 . Similar to the analysis of the transmit antenna gain, the receive antenna gain is equal to the main lobe gain with the hitting probability $p_U = p_{U,V} p_{U,H}$, where $p_{U,V}$ and $p_{U,H}$ are the probabilities that the interfering AP is within the vertical and horizontal beams of U_0 , respectively. As shown in [10, Fig. 6(a)], the vertical beam range of U_0 is determined by the maximum horizontal distance $R_{U_0,\text{max}}$, which is calculated as

$$R_{U_0,\text{max}} = \frac{h_A - h_U}{\tan \left(\arctan \left(\frac{h_A - h_U}{d_0} \right) - \frac{\phi_{U,V}}{2} \right)}. \quad (14)$$

An interfering AP, AP_i , is within the vertical beam of U_0 if its distance to U_0 , d_i , is less than or equal to $R_{U_0,\text{max}}$. For the horizontal beam of U_0 , based on the properties of the PPP, we have $p_{U,H} = \frac{\phi_{U,H}}{2\pi}$. By combining $p_{U,V}$ and $p_{U,H}$, we obtain the hitting probability of an interfering AP, AP_i , within the antenna beam of U_0 .

Based on our analysis of both transmit and receive antenna gains, the probability distribution of the antenna gain for AP_i is given by

$$\Pr(G_i) = \begin{cases} p_A p_U, & \text{if } G_i = G_{A,m} G_{U,m}, \\ p_A (1 - p_U), & \text{if } G_i = G_{A,m} G_{U,s}, \\ (1 - p_A) p_U, & \text{if } G_i = G_{A,s} G_{U,m}, \\ (1 - p_A) (1 - p_U), & \text{if } G_i = G_{A,s} G_{U,s}. \end{cases} \quad (15)$$

C. Coverage Performance Analysis

Building on the derived $f_{H_{pe}}(h_{pe})$, $f_{D_0}(d_0)$, and antenna gain analysis for interference signals, we now derive the coverage probability and present it in the following Theorem.

Theorem 1: The coverage probability of U_0 is derived as

$$P_c = \int_0^\infty \int_0^1 f_{H_{pe}}(h_{pe}) \Gamma(m) \sum_{j=0}^\infty \frac{(\mu K)^j r_j}{\Gamma(j+1)} \sum_{l=0}^{j+\mu-1} \frac{(-s)^l}{l!} \times \left. \frac{\partial^{(l)} \mathcal{L}_{I+N_0}(s|h_{pe}, d_0)}{\partial s^l} \right|_{s=\rho} f_{D_0}(d_0) dh_{pe} dd_0, \quad (16)$$

where $\rho = \frac{(j+\mu)\gamma_{\text{th}}}{2\sigma^2 P_t \xi G_{\max} h_{pe} W(d)}$ and

$$\begin{aligned} \mathcal{L}_{I+N_0}(s|h_{pe}, d_0) &= \exp \left(-s N_0 - \int_{d_0}^\infty \Lambda_{A,\text{LoS}}(d) \sum_{G_i} \Pr(G_i) \right. \\ &\times \left. \left(\frac{m^m}{\Gamma(m)} \sum_{j=0}^\infty \frac{(\mu K)^j r_j}{j! (1 + 2s\sigma^2 P_t \xi G_i W(d))^{j+\mu}} \right) dd \right) \end{aligned} \quad (17)$$

represents the Laplace transform of the interference plus noise power.

Proof: We note that the coverage probability can be calculated by

$$P_c = \int_0^\infty \int_0^1 \Pr \left(\frac{P_t \xi G_{\max} h_{pe} W(d_0) H_{S,0}}{I + N_0} > \gamma_{\text{th}} \middle| h_{pe}, d_0 \right) \times f_{H_{pe}}(h_{pe}) f_{D_0}(d_0) dh_{pe} dd_0. \quad (18)$$

Using the CDF of $H_{S,0}$ in (3), the conditional coverage probability in (18) is expressed as

$$\begin{aligned} & \Pr \left(\frac{P_t \xi G_{\max} h_{pe} W(d_0) H_{S,0}}{I + N_0} > \gamma_{\text{th}} \middle| h_{pe}, d_0 \right) \\ &= \mathbb{E}_I \left[\frac{m^m}{\Gamma(m)} \sum_{j=0}^{\infty} \frac{(\mu K)^j r_j}{\Gamma(j+1)} \sum_{l=0}^{j+\mu-1} \frac{(\rho(I + N_0))^l}{l!} e^{-\rho(I + N_0)} \right] \\ &= \frac{m^m}{\Gamma(m)} \sum_{j=0}^{\infty} \frac{(\mu K)^j r_j}{\Gamma(j+1)} \sum_{l=0}^{j+\mu-1} \frac{(-s)^l \partial^{(l)} \mathcal{L}_{I+N_0}(s|h_{pe}, d_0)}{\partial s^l} \Big|_{s=\rho}. \quad (19) \end{aligned}$$

According to the property of the PPP, we calculate $\mathcal{L}_{I+N_0}(s|h_{pe}, d_0)$ in (19) as

$$\begin{aligned} \mathcal{L}_{I+N_0}(s|h_{pe}, d_0) &= e^{-sN_0} \mathbb{E} \left[\exp \left(-s \sum_{AP_i \in \Psi_{AP}} P_i \right) \middle| d_0 \right] \\ &= \exp \left(-sN_0 - \int_{d_0}^{\infty} (1 - \mathbb{E}[\exp(-sP_i)]) \Lambda_{A, \text{LoS}}(d) dd \right), \quad (20) \end{aligned}$$

where $\mathbb{E}[\exp(-sP_i)]$ is computed as

$$\begin{aligned} \mathbb{E}[\exp(-sP_i)] &= \sum_{G_i} \Pr(G_i) \\ &\times \left(\frac{m^m}{\Gamma(m)} \sum_{j=0}^{\infty} \frac{(\mu K)^j r_j}{j! (1 + 2s\sigma^2 P_t \xi G_i W(d))^{j+\mu}} \right). \quad (21) \end{aligned}$$

By substituting (17) into (19) and combining it with (18), we obtain the coverage probability of U_0 as (16). ■

From Theorem 1, we find that the pointing error has a significant impact on the coverage performance. This impact can be addressed by employing technologies that enhance angle-of-arrival detection, enabling more accurate estimation of the UE's location. This improved estimation leads to more precise antenna alignment, which in turn increases the received signal power and ultimately enhances the coverage probability.

IV. NUMERICAL RESULTS

In this section, we first present numerical results to verify our analysis in Section III and evaluate the impact of various parameters on the coverage probability, such as the standard deviation of the estimated angle error and the number of antennas at the AP and UE. The values of the parameters used in this section are summarized in Table I, unless specified otherwise.

Fig. 2 plots the PDF of the pointing error loss, $f_{H_{pe}}(h_{pe})$. We first observe that our analytical results in Lemma 1 align well with the simulation results, validating the correctness of

TABLE I
VALUE OF SYSTEM PARAMETERS USED IN SECTION IV.

Parameter	Symbol	Value
Operating frequency	f	0.3 THz
Absorption coefficient	$\epsilon(f)$	0.00143 m^{-1}
Height of APs and UEs	h_A, h_U	3 m, 1 m
Height and radius of human	h_B, R_B	1.7 m, 0.25 m
Density of APs and human	λ_A, λ_B	$0.1 \text{ m}^{-2}, 0.1 \text{ m}^{-2}$
Density and length of wall	$\lambda_W, \mathbb{E}[L_W]$	$0.04 \text{ m}^{-2}, 3 \text{ m}$
Transmit and AWGN power	P_t, N_0	5 dBm, -77 dBm
Antenna parameters	N_A, N_U, R_A	16, 4, 15 m
MFTR fading parameters	K, m, Δ, μ	5, 2, 0.3, 2

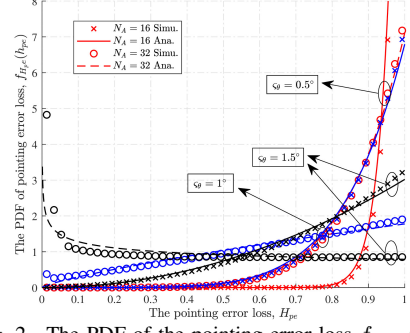


Fig. 2. The PDF of the pointing error loss $f_{H_{pe}}(h_{pe})$.

our analysis. We then observe that this PDF for $N_A = 32$ is larger than that for $N_A = 16$ when H_{pe} is small, but smaller when H_{pe} is large. This is due to the fact that a larger number of antennas results in a narrower main lobe, which increases the likelihood of a smaller pointing error loss compared to the case with fewer antennas. This observation also indicates that the average pointing error loss decreases when the number of antennas increases, highlighting the importance of accurate location estimation in THz communication systems with large antenna arrays.

Fig. 3 plots the coverage probability, P_c , versus the SINR threshold, γ_{th} , for various ς_θ . We first observe that our analytical results in Theorem 1 align well with the simulation results, especially for small ς_θ , confirming the accuracy of our analysis. We note that there is a small gap between the simulation and the analytical results for $\varsigma_\theta = 1.5^\circ$ at low SNR thresholds. This gap is caused by the approximation of the main lobe gain using a Gaussian beam model, which neglects side lobe gain. This small side lobe gain can noticeably affect the coverage probability at low SNR thresholds and lead to a mismatch between analytical and simulation results. We then observe that when $\varsigma_\theta = 0$, the coverage probability is almost identical for two antenna configurations, namely, $N_A = 16$ with $N_U = 8$ and $N_A = 32$ with $N_U = 4$. However, when $\varsigma_\theta = 1.5^\circ$, a significant difference in P_c emerges between these two configurations. This observation supports the insights from Remark 1, as it reveals that while the maximum antenna gain is the same for both configurations, a larger antenna array, such as $N_A = 32$, results in a narrower beam. This narrower beam makes the system more sensitive to the estimated angle error, leading to a more substantial degradation in P_c as ς_θ increases.

Fig. 4 plots the coverage probability, P_c , versus the antenna array size of AP, N_A , with the SINR threshold $\gamma_{\text{th}} = 30 \text{ dB}$.

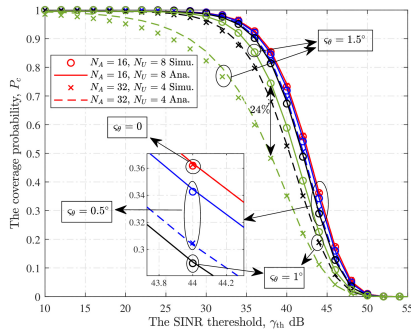


Fig. 3. The coverage probability, P_c , versus the SINR threshold, γ_{th} dB.

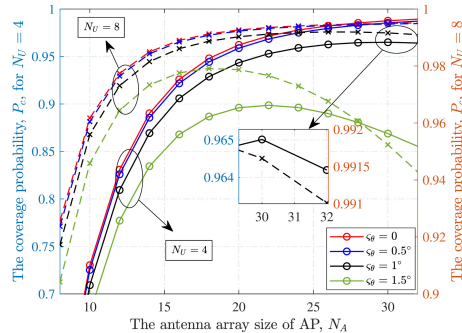


Fig. 4. The coverage probability, P_c , versus the antenna array size of AP, N_A , with the SINR threshold $\gamma_{th} = 30$ dB.

We observe that for $s_\theta = 0$, P_c increases monotonically with N_A . However, when $s_\theta \neq 0$, P_c initially increases and then decreases as N_A increases, particularly when ϑ is large. This observation is due to the fact that as N_A increases, the antenna gain of the AP improves, enhancing the received signal power. However, as N_A continues to increase, the beamwidth of the AP decreases, which in turn increases the side lobe gain, leading to a higher interference power. This effect is more pronounced as s_θ increases. This observation implies that the coverage probability is fundamentally constrained by the pointing error and cannot be indefinitely improved by simply increasing the antenna array size. In addition, it highlights the critical role of accurate location estimation in enhancing the coverage performance in THz communication systems.

V. CONCLUSION

We developed a tractable analytical framework to evaluate the impact of pointing error on the coverage performance of indoor THz communication systems. We derived a new expression for the coverage probability of the typical UE, incorporating both the small-scale fading and pointing error. Through numerical results, we first verified our analysis and examined how the pointing error affects the received signal power at the UE. We then evaluated the joint impact of the pointing error and the antenna array size on the coverage probability. Our results quantified the degradation caused by the pointing error in the coverage probability, highlighting the critical importance of accurate pointing in THz systems. Furthermore, we demonstrated that merely increasing the antenna array size is insufficient to enhance coverage performance. These findings highlight the necessity of adopting accurate

location estimation techniques to optimize performance in indoor THz communication systems.

ACKNOWLEDGMENT

This work was funded by the Australian Research Council Discovery Project DP230100878.

REFERENCES

- [1] M. Giordani, M. Polese, M. Mezzavilla, S. Rangan, and M. Zorzi, "Toward 6G networks: Use cases and technologies," *IEEE Commun. Mag.*, vol. 58, no. 3, pp. 55–61, Mar. 2020.
- [2] N. Yang and A. Shafie, "Terahertz communications for massive connectivity and security in 6G and beyond era," *IEEE Commun. Mag.*, vol. 62, no. 2, pp. 72–78, Feb. 2024.
- [3] Z. Tang, N. Yang, X. Zhou, S. Durrani, M. Juntti, and J. M. Jornet, "Low complexity artificial noise aided beam focusing design in near-field terahertz communications," Feb. 2025. [Online]. Available: <https://arxiv.org/abs/2502.08967>
- [4] J. M. Jornet and I. F. Akyildiz, "Channel modeling and capacity analysis for electromagnetic wireless nanonetworks in the terahertz band," *IEEE Trans. Wireless Commun.*, vol. 10, no. 10, pp. 3211–3221, Oct. 2011.
- [5] K. Venugopal and R. W. Heath, "Millimeter wave networked wearables in dense indoor environments," *IEEE Access*, vol. 4, pp. 1205–1221, Mar. 2016.
- [6] V. Petrov, M. Komarov, D. Moltchanov, J. M. Jornet, and Y. Koucheryavy, "Interference and SINR in millimeter wave and terahertz communication systems with blocking and directional antennas," *IEEE Trans. Wireless Commun.*, vol. 16, no. 3, pp. 1791–1808, Mar. 2017.
- [7] Y. Wu, J. Kokkoniemi, C. Han, and M. Juntti, "Interference and coverage analysis for terahertz networks with indoor blockage effects and line-of-sight access point association," *IEEE Trans. Wireless Commun.*, vol. 20, no. 3, pp. 1472–1486, Mar. 2021.
- [8] A. Shafie, N. Yang, S. Durrani, X. Zhou, C. Han, and M. Juntti, "Coverage analysis for 3D terahertz communication systems," *IEEE J. Select. Areas Commun.*, vol. 39, no. 6, pp. 1817–1832, Jun. 2021.
- [9] N. Kouzayha, M. A. Kishk, H. Sarieddeen, M.-S. Alouini, and T. Y. Al-Naffouri, "Coexisting terahertz and RF finite wireless networks: Coverage and rate analysis," *IEEE Trans. Wireless Commun.*, vol. 22, no. 7, pp. 4873–4889, Jul. 2023.
- [10] Z. Tang, N. Yang, S. Durrani, X. Zhou, M. Juntti, and J. M. Jornet, "Coverage analysis for 3D indoor terahertz communication system over multi-cluster fluctuating two-ray fading channels," *IEEE Trans. Commun.*, pp. 1–1, May 2025.
- [11] A.-A. A. Boulogeorgos, J. M. Riera, and A. Alexiou, "On the joint effect of rain and beam misalignment in terahertz wireless systems," *IEEE Access*, vol. 10, pp. 58 997–59 012, Jun. 2022.
- [12] V. Petrov, D. Moltchanov, Y. Koucheryavy, and J. M. Jornet, "Capacity and outage of terahertz communications with user micro-mobility and beam misalignment," *IEEE Trans. Veh. Technol.*, vol. 69, no. 6, pp. 6822–6827, Jun. 2020.
- [13] M. T. Dabiri and M. Hasna, "Pointing error modeling of mmWave to THz high-directional antenna arrays," *IEEE Wireless Commun. Lett.*, vol. 11, no. 11, pp. 2435–2439, Nov. 2022.
- [14] E. Safahan Ahrazoglu, A. Caner Gul, M. Nuri Akinci, I. Altunbas, and E. Erdogan, "An improved pointing error model for mmWave and THz links: Antenna and array design impact," *IEEE Commun. Lett.*, vol. 29, no. 3, pp. 532–536, Mar. 2025.
- [15] M. T. Dabiri, M. Hasna, N. Zorba, and T. Khattab, "Optimal trajectory and positioning of UAVs for small cell HetNets: Geometrical analysis and reinforcement learning approach," *IEEE Open J. Commun. Soc.*, vol. 4, pp. 2667–2683, Oct. 2023.
- [16] H. Yuan, N. Yang, K. Yang, C. Han, and J. An, "Hybrid beamforming for terahertz multi-carrier systems over frequency selective fading," *IEEE Trans. Commun.*, vol. 68, no. 10, pp. 6186–6199, Oct. 2020.
- [17] E. Papasotiriou, A.-A. Boulogeorgos, K. Haneda, M. F. De Guzman, and A. Alexiou, "An experimentally validated fading model for THz wireless systems," *Sci. Rep.*, vol. 11, Sep. 2021.
- [18] J. D. V. Sánchez, F. J. Lopez-Martinez, J. F. Paris, and J. M. Romero-Jerez, "The multi-cluster fluctuating two-ray fading model," *IEEE Trans. Wireless Commun.*, vol. 23, no. 5, pp. 4199–4213, May 2024.
- [19] P. Gerstoft, C. F. Mecklenbräuker, A. Xenaki, and S. Nannuru, "Multisnapshot sparse bayesian learning for DOA," *IEEE Signal Process. Lett.*, vol. 23, no. 10, pp. 1469–1473, Oct. 2016.